Supporting Information

Zhang et al. 10.1073/pnas.1218699110

SI Experimental Procedures

Immunohistochemistry. Brains were dissected at the indicated time points and frozen immediately. Sections (14-μm) were cut through the entire brain using a cryostat (Zeiss). Sections were mounted onto glass slides and incubated with rabbit anti-PKCγ C-19 (1:1,000; Santa Cruz). The sections were subsequently processed with the avidin–biotin–immunoperoxidase technique using diaminobenzidine (DAB) as the chromagen.

Quantitative Real-Time RT-PCR. Brains were dissected at the indicated time points and placed in a rodent brain matrix (RBM2000C; ASI Instruments). Slices starting from the rostral end of the brain and ending at the appearance of ventral hippocampal commissure (Bregma –0.2 mm) were obtained and the cortical regions were dissected. Tissues were immediately frozen until total RNA was extracted using TRIzol (Invitrogen). Quantitative PCR analysis was performed using the QuantiTect SYBR Green One-Step RT-PCR Kit (Qiagen). Primers used were as previously reported (1).

1. Yamamoto T, et al. (2004) Transcriptional oscillation of canonical clock genes in mouse peripheral tissues. *BMC Mol Biol* 5(1):18.

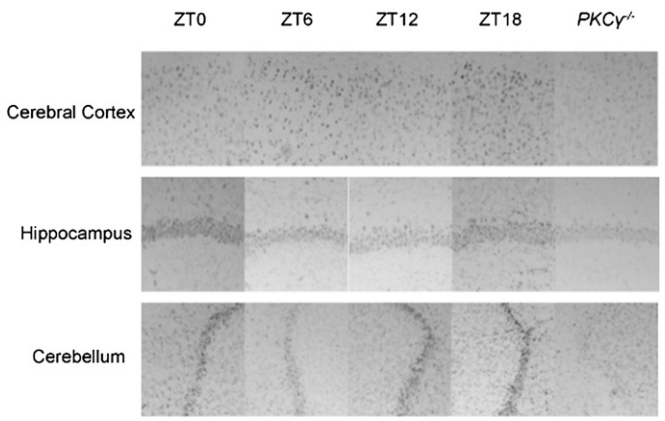

Fig. S1. PKCγ is prominently expressed in food-entrainable brain regions. Immunostaining with PKCγ antibody in the cerebral cortex, hippocampus, and cerebellum of WT and $PKC\gamma^{-/-}$ mice under 12-h light/12-h dark (12L12D) conditions. ZT, Zeitgeber time.

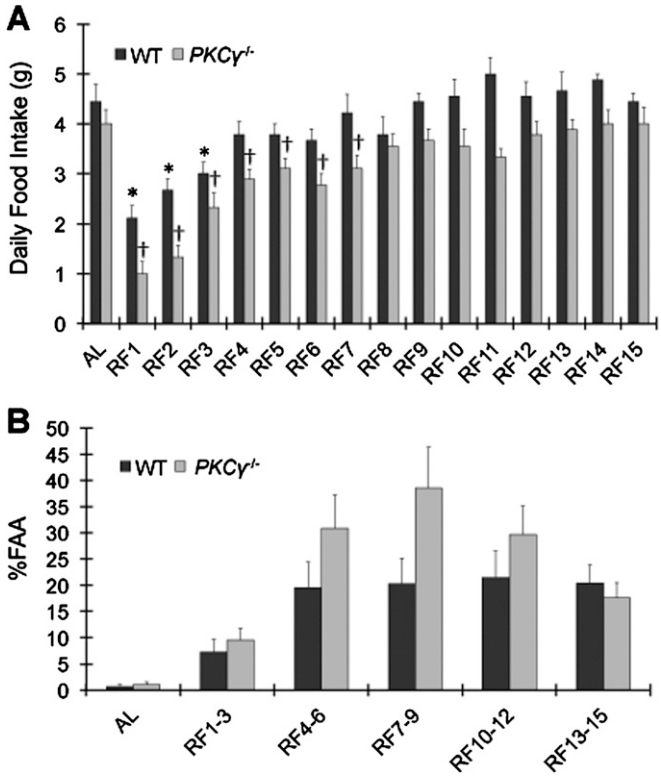

Fig. S2. *PKCγ*$^{-/-}$ mice entrain to food. (*A*) Mean food intake during food ad libitum (AL) and temporally restricted feeding (RF) of WT and *PKCγ*$^{-/-}$ mice ($n = 9$). Asterisks mark significant differences between RF and AL for WT (Student's *t* test, $^{*}P < 0.05$), whereas daggers mark significant differences between RF and AL for *PKCγ*$^{-/-}$ (Student's *t* test, $^{\dagger}P < 0.05$). (*B*) Three-hour (ZT3–ZT6) food-anticipatory activity (FAA) displayed as the percentage of total activity in WT and *PKCγ*$^{-/-}$ mice during AL and 15 d of RF under 12L12D conditions ($n = 8$). Error bars represent SEM.

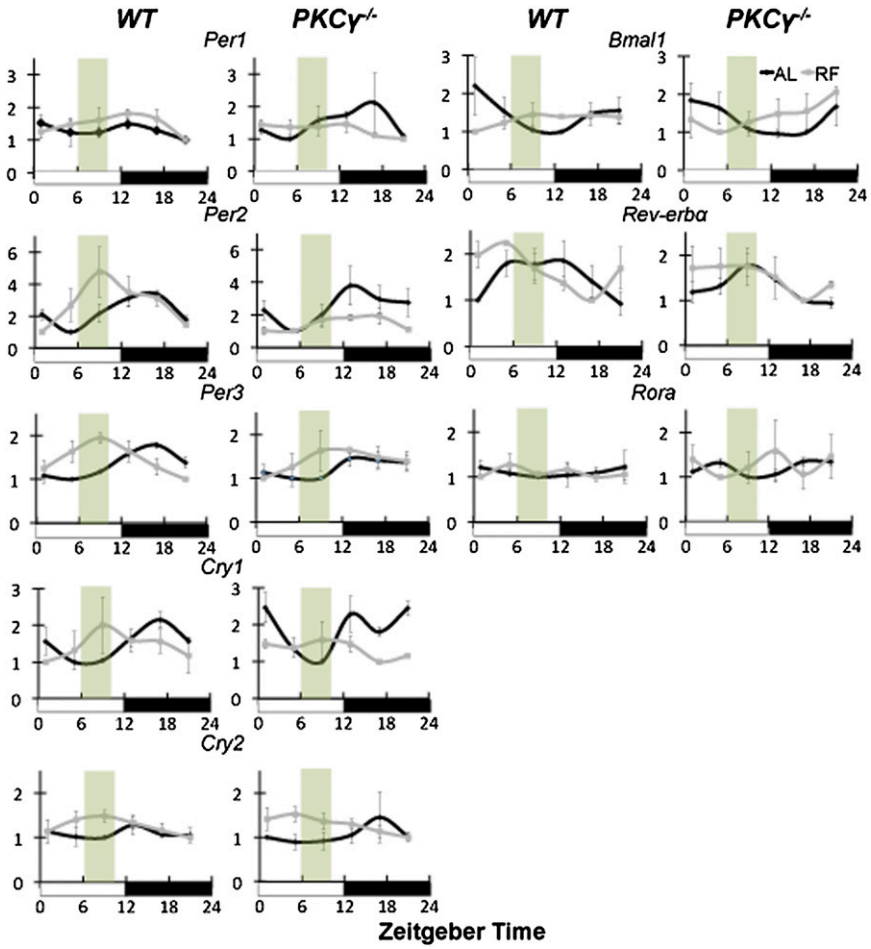

Fig. S3. Restricted feeding substantially phase resets the cycling of clock gene transcripts in the cerebral cortex of wild-type but not $PKC\gamma^{-/-}$ mice. Plots of relative mRNA abundance vs. ZT for each core clock gene in the cerebral cortex of WT and $PKC\gamma^{-/-}$ mice during AL and on RF day 2 determined by quantitative real-time RT-PCR. Averaged values are shown as dark gray data points for AL and light gray data points for RF. Error bars represent SEM (n = 3). Significant treatment X ZT interaction (two-way repeated measures ANOVA) for *Per2* of WT (P = 0.0376), *Per3* of WT (P < 0.0001), *Cry1* of WT (P = 0.0144), *Bmal1* of WT (P = 0.0162), *Rev-erbα* of WT (P = 0.0054), and *Cry1* of $PKC\gamma^{-/-}$ (P = 0.0135). For each time series, the value of the lowest time point was set to 1. The white and black boxes indicate light regime, whereas food availability during RF is indicated by the green shading.

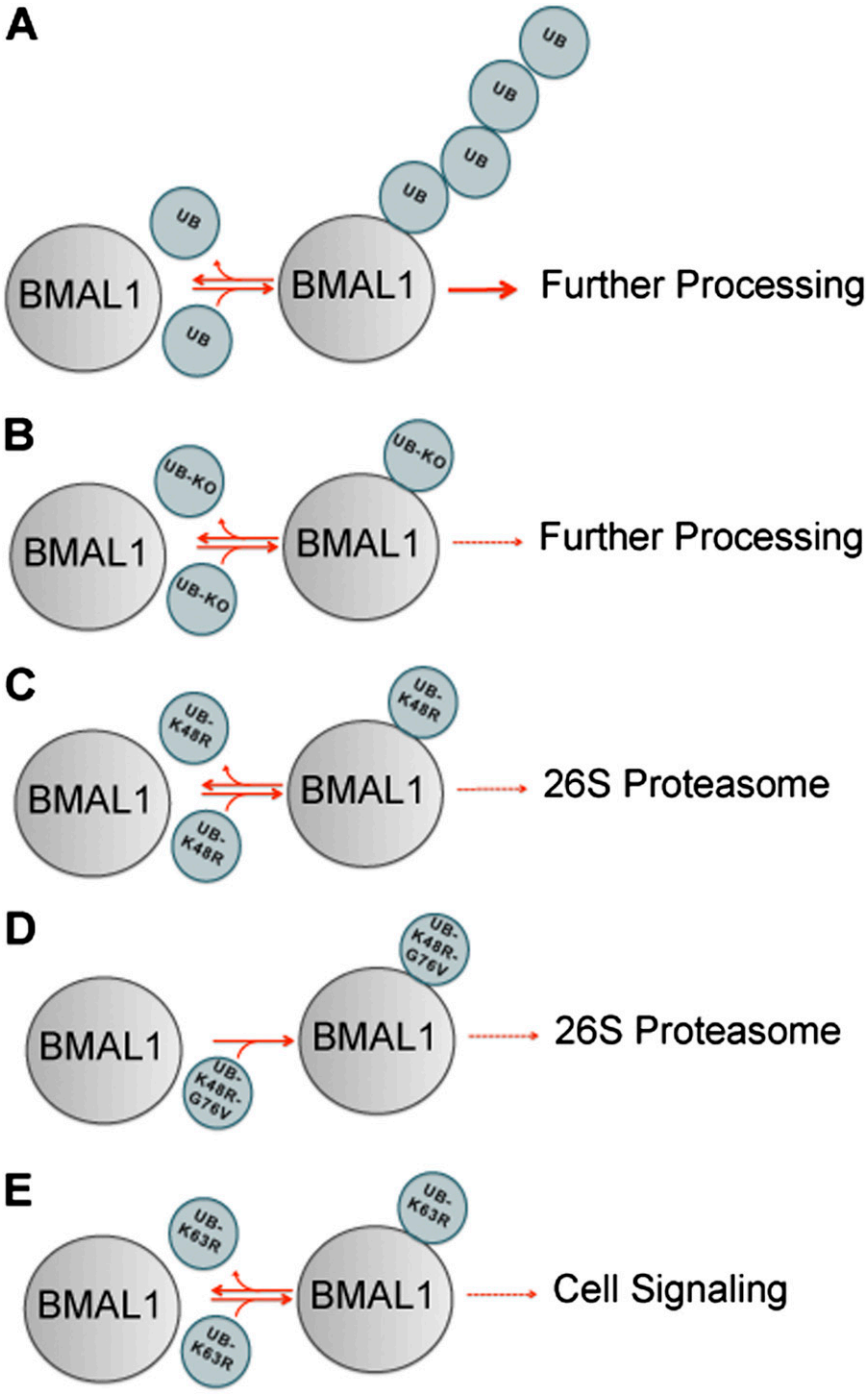

Fig. S4. Schematic demonstrating the consequences of various ubiquitin mutations. (*A*) WT ubiquitin can be conjugated to BMAL1 and form a polyubiquitin chain targeting BMAL1 for further processing. It can also be cleaved off from BMAL1. (*B*) When conjugated to BMAL1, UB-KO prevents further assembly of ubiquitin chain and thus BMAL1 cannot be further processed. (*C*) When conjugated to BMAL1, UB-K48R mutant blocks formation of ubiquitin chain assembled through the K48 position and thus prevents BMAL1 degradation by 26S proteasome. (*D*) When conjugated to BMAL1, UB-K48R-G76V not only blocks formation of ubiquitin chain assembled through K48 and thus 26S proteasome-mediated degradation of BMAL1 but also prevents ubiquitin cleavage from BMAL1 or deubiquitination of BMAL1. (*E*) When conjugated to BMAL1, UB-K63R blocks formation of ubiquitin chain assembled through K63 and thus prevents subsequent cell-signaling events.

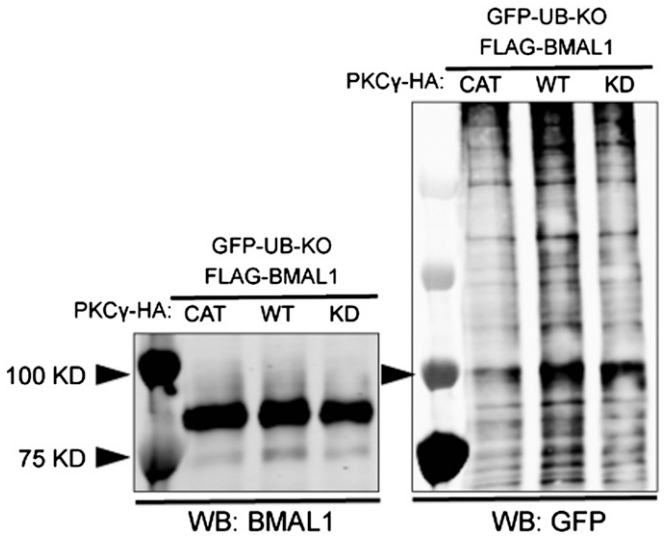

Fig. S5. PKCγ reduces total ubiquitylation of BMAL1. FLAG-BMAL1, GFP-UB-KO, and different forms of PKCγ [constitutively active (CAT), WT, or kinase-dead (KD)] were coexpressed in HEK293T cells. FLAG-BMAL1 was immunoprecipitated from cell lysates; BMAL1 and GFP-UB-KO were detected in the same Western blot (WB) in the immunoprecipitated proteins with antibodies as specified.

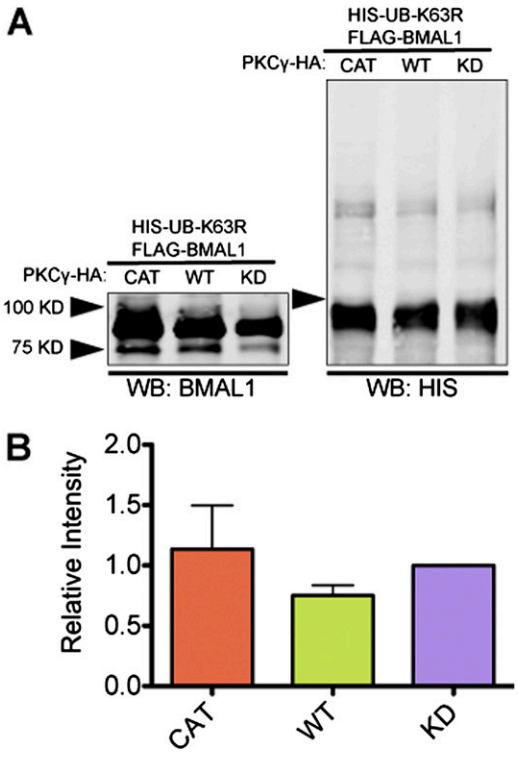

Fig. S6. PKCγ does not reduce K63-mediated ubiquitylation of BMAL1. (*A*) FLAG-BMAL1, HIS-UB-K63R, and different forms of PKCγ (CAT, WT, or KD) were coexpressed in HEK293T cells. FLAG-BMAL1 was immunoprecipitated from cell lysates; BMAL1 and HIS-UB-K63R were detected in the same Western blot in the immunoprecipitated proteins with antibodies as specified. (*B*) Bar graph showing quantification of Western blots in *A* (n = 2–3). HIS-UB-K63R levels were normalized to the amount of FLAG-BMAL1 pulled down, and the amount of His-UB-K63R in cells transfected with PKCγKD was set to 1. Error bars represent SEM.

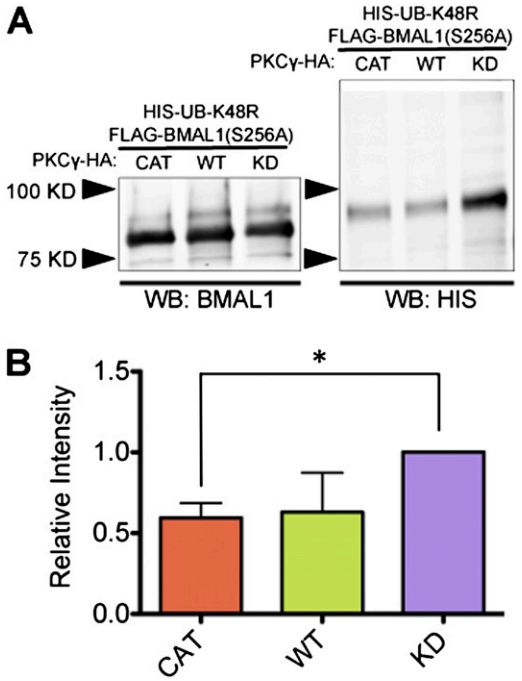

Fig. S7. BMAL1-S256A mutation does not eliminate the effects of PKCγ on BMAL1 ubiquitylation. (*A*) FLAG-BMAL1-S256A, HIS-UB-K48R, and different forms of PKCγ (CAT, WT, or KD) were coexpressed in HEK293T cells. FLAG-BMAL1-S256A was immunoprecipitated from cell lysates; BMAL1-S256A and HIS-UB-K48R were detected in the same Western blot in the immunoprecipitated proteins with antibodies as specified. (*B*) Bar graph showing quantification of Western blots in *A* ($n = 3–4$). HIS-UB-K48R levels were normalized to the amount of FLAG-BMAL1 pulled down, and the amount of HIS-UB-K48R in cells transfected with PKCγKD was set to 1. Error bars represent SEM. Asterisks marks significant differences between the two groups (Student's *t* test, $*P < 0.05$).